

● *Original Contribution*

QUANTITATIVE ULTRASONIC METHODS FOR CHARACTERIZATION OF SKIN LESIONS *IN VIVO*

BALASUNDAR I. RAJU,* KIRSTY J. SWINDELLS,[†] SALVADOR GONZALEZ[†] and
MANDAYAM A. SRINIVASAN*

*Laboratory for Human and Machine Haptics, Research Laboratory of Electronics, Massachusetts Institute of Technology, Cambridge, MA, USA; and [†]Wellman Laboratories of Photomedicine, Department of Dermatology, Massachusetts General Hospital, Boston, MA, USA

(Received 6 June 2002; in final form 20 December 2002)

Abstract—Quantitative ultrasonic methods were studied for characterizing skin lesions *in vivo* using contact dermatitis as an example. The parameters studied include skin thickness, echogenicity, attenuation coefficient slope and parameters related to echo statistics (signal-to-noise ratio and shape parameters of Weibull, K and generalized gamma distributions). Data were collected using a high-frequency ultrasound (US) system (center frequency = 33 MHz). To compensate for depth-dependent diffraction effects, correction curves as a function of the distance between the transducer and the tissue were first empirically obtained. Diffraction-corrected quantitative parameters were then compared between healthy and affected skin of volunteers, who underwent patch testing for allergic and irritant contact dermatitis. A significant increase in skin thickness, decrease in echogenicity of the upper dermis and decrease in attenuation coefficient slope were found at the affected sites compared to those of healthy skin. However, no differences in parameters related to the echo statistics of the mid-dermis were found. These results indicate that a combination of quantitative ultrasonic parameters have the potential for extracting information for characterizing skin conditions. (E-mail: raju@alum.mit.edu) © 2003 World Federation for Ultrasound in Medicine & Biology.

Key Words: High-frequency ultrasound, Skin, Dermis, Tissue characterization, Diffraction compensation, Attenuation coefficient, Echogenicity, Echo statistics, Dermatology, Contact dermatitis.

INTRODUCTION

Quantitative ultrasonic tissue parameters, such as the attenuation coefficient, backscatter coefficient, mean size of scatterers, scatterer number density and echo statistics, have been widely studied for their potential to classify normal vs. abnormal conditions in several tissues including the heart, liver, spleen, breast, eye and kidney (Insana et al. 1986; Shung and Thieme 1993; Molthen et al. 1998). These methods, referred to as quantitative ultrasonic methods or tissue-characterization methods, are undertaken because of the fact that ultrasound (US) B-scan images utilize only partial information in the back-scattered echoes and, through appropriate signal processing, additional parameters that provide information about tissue pathologies could be extracted. In the case of skin tissues, such studies have not been widely investigated

for characterizing skin lesions, despite the increasing reliance of high-frequency (≥ 20 MHz) US as a noninvasive imaging tool. Although US has the capability to image fine features in the skin, such as sweat gland ducts, hair follicles and veins, the diagnostic capabilities of skin images to identify specific pathologies are limited (Foster et al. 2000). For instance, it is difficult to differentiate between benign and malignant lesions using B-scan images (Fornage et al. 1993) because both types of lesions appear hypoechogenic with respect to healthy skin. Another study indicated that both scar tissue and malignant melanoma could appear similar in US scans (Turnbull et al. 1995). Given the fact that skin is affected by a large number of lesions, it is worthwhile to study if tissue-characterization methods have the potential to extract additional information for identifying and classifying various skin lesions.

Previous quantitative studies of skin lesions *in vivo* using US have mostly been limited to parameters that could be computed directly from images obtained using

Address correspondence to: Balasundar I. Raju, Ph.D., Philips Research, 345 Scarborough Road, Briarcliff Manor, NY 10510. E-mail: raju@alum.mit.edu

commercially available 20-MHz systems. For instance, changes in skin echogenicity (mean pixel amplitude, which is proportional to the mean backscatter amplitude) and skin thickness were found to be related to photoaging of the skin (Gniadecka and Jemec 1998). The degree of acoustic shadowing, measured as the ratio of echogenicity of the retrolesional dermis to that of the perilesional dermis, was found to be capable of differentiating between basal cell papilloma and malignant melanoma (Harland et al. 2000). Other parameters that require analysis of the radiofrequency (RF) backscattered echoes, such as the attenuation coefficient (Guittet et al. 1999) and apparent integrated backscatter (Fournier et al. 2001) have also been studied in healthy skin tissues *in vivo*. In our earlier work, we have studied the frequency-dependent attenuation and backscatter coefficients (Raju and Srinivasan 2001), as well as parameters related to echo statistics, such as the ratio of mean to SD, denoted as signal-to-noise ratio (SNR) and parameters of envelope probability density functions (pdfs) of healthy skin tissues *in vivo* (Raju and Srinivasan 2002).

The purpose of the present study was to develop quantitative ultrasonic methods free of diffraction effects that could be used in a clinical research setting in dermatology, and to test the methods with an example, namely, contact dermatitis. The computation of quantitative parameters requires compensation for the system-dependent effects because the recorded signals are dependent both on the tissue, as well as the instrument used in recording the signals. For instance, when focused transducers are used, variations in beam amplitude due to depth-dependent diffraction effects could affect the attenuation and backscatter coefficients (Madsen 1993). Also, variations in beam size along the path of the beam would lead to changes in the number of scatterers contributing to the resultant echo signal from the tissue, thereby affecting the echo statistics (Tuthill et al. 1988). Diffraction compensation curves obtained empirically using reflections from a plane reflector placed at several distances from the transducer are only approximately helpful because the correction function depends on the tissue being imaged (Robinson et al. 1984). In practice, it has been found that shifting the location of the transducer's focal zone so as to always position it at the region-of-interest (ROI) is a more reliable way to compensate for the diffraction effects (Ophir and Mehta 1988). Such a method, when applied to quantitative US at high frequencies (> 20 MHz) poses special considerations because phased-array transducers at high frequencies are not currently available and mechanically scanned single-element transducers are commonly used. The speed of data collection is limited by the scan velocity, which is, at best, a few mm/s. Also, unlike in conventional US (1 to 10 MHz), the tolerances in high-frequency US are

much higher, and motion artefacts of even a small fraction of a mm during data collection are undesirable. When data from several focal zone locations are needed, the transducer must be mechanically moved toward the tissue and the scans must be repeated. The total time of imaging is, thus, increased and only body sites that are can be held stationary using braces (*e.g.*, forearm) can be studied. Therefore, a more reliable way to compensate for diffraction is needed. It should be noted that combining several B-scans with the transducer being moved toward the tissue between the scans has been previously used in skin imaging (Passmann and Ermer 1996). The individual B-scans, which have an axial dimension equal to the depth of focus of the transducer, are combined into one composite B-scan. However, in the case of quantitative studies, data corresponding to a much larger number of such depths are needed. This is because the depth of focus is a distance based on -6 dB variations in the beam amplitude, which might be large enough to offset changes in signal levels due to attenuation within that same distance. Hence, axially translating the transducer by a distance equal to the depth of focus is not sufficient, and a much closer spacing between the locations of the focal zones are required. This, in turn, leads to the problem of increased time of imaging and motion artefacts.

In light of the above comments, we first decided to empirically determine diffraction correction curves using the healthy skin of several human volunteers. These experiments were done on a convenient location on the forearm, which could be held stationary during the experiment with prior planning. Data collected from 19 locations of the focal zone through axial translation were obtained to determine changes in quantitative measures as a function of distance from the transducer. The correction curves were obtained for both the beam amplitude as a function of frequency and for parameters related to the echo statistics. The correction curves were then tested on one independent subject. Finally, to demonstrate the application of the methods, the capability of the quantitative methods to distinguish between contact dermatitis and healthy skin was studied. Contact dermatitis is an inflammatory skin condition caused by skin contact with an exogenous agent. It can be broadly classified into two types, allergic and irritant. Both these types were studied and compared with healthy skin tissues without regard to the particular type. The reason for studying contact dermatitis was that it was easy to induce the condition in volunteers using standard patch-testing methods. Quantitative parameters, namely, skin thickness, echogenicity, attenuation coefficient and parameters related to the echo statistics were studied for their capability to differentiate between contact dermatitis and healthy skin.

Table 1. Characteristics of the transducer used in this study

Transducer	Panametrics PI50*
Center frequency	33 MHz
-6 dB BW	28 MHz
F-number	2
Focal length	12.7 mm
Diameter	6.35 mm
-6 dB Depth of focus	1.3 mm
Axial resolution	25 μm
Lateral resolution	90 μm

*Pulser setting: energy = 4 μJ ; damping = 50 Ω . The axial and lateral resolutions were computed based on theoretical expressions for the -6 dB full widths.

MATERIALS AND METHODS

Experimental system

The high-frequency imaging system used in this work was a modified version of an earlier system described in a previous work (Raju and Srinivasan 2001). The present system consisted of a PVDF transducer (Panametrics, Waltham, MA; model PI50), a pulser/receiver (Panametrics; model PR5900), a three-axis scanning system (Compumotor/Parker-Hannifin, Cleveland, OH), and a high-speed PCI-bus based A/D board (Gage Applied Sciences, Montreal, Canada; model Compuscope 8500). The transducer characteristics (center frequency and BW) were found to be dependent on the pulser energy and damping settings, which were set to 4 μJ and 50 ohms, respectively. Table 1 shows the system characteristics. The vertical range on the A/D converter was set to record signals between -0.5 and 0.5 volts, which was found to be optimal to acquire backscatter echoes from the dermis, although the surface echo was sometimes saturated. The sampling frequency of the A/D board was chosen to be 200 MHz. The main improvement in the system from the earlier system mentioned in Raju and Srinivasan (2001) was the use of the Gage data-acquisition board instead of the digitizing oscilloscope, which enabled much faster data transfer rates from the digitizer to the PC memory. This, in turn, made it possible to perform a continuous scan of the transducer wherein the echo lines (RF lines corresponding to A-scans) could be recorded and stored in the PC memory by acquiring data at regular intervals while the transducer was moving. The transducer was set to scan continuously at a constant speed of 2 mm/s. The echo lines, separated by a spacing of 25 μm , were recorded by acquiring data at a time interval of 12.5 ms between the lines. To improve the SNR, each recorded echo line was, itself, an average of 50 repeated echoes, all acquired in rapid succession when the transducer was in a continuous scan. This was possible because the distance traversed by the transducer during the period corresponding

to all the 50 echoes was much smaller than the lateral resolution of the system, explained as follows: The PRF of the pulser was 20 kHz, which corresponded to an interpulse period of 50 μs . Therefore, the total duration for all the 50 echoes that made up a single echo line was 50 $\mu\text{s/pulse} \times 50 \text{ pulses} = 2.5 \text{ ms}$. Hence, for a scanning speed of 2 mm/s, this duration corresponded to a distance of 2 mm/s \times 2.5 ms = 5 μm , which was only about 6% of the system's lateral resolution. Such a data acquisition proceeded until the total scan length was covered, which was typically 5 mm. The space between the transducer and the body site being imaged was filled with distilled water, using a small water cup with a slot to allow the US beam to pass through.

Data collection

During an experiment, several B-scans as described above were done. The reasons for performing several scans were twofold: First, a skin lesion is spread out laterally over an area, whereas a single B-scan will only cover one slice through the lesion. Hence, additional scans were done after translating the transducer laterally in a direction perpendicular to the scan direction. Second, because a single diffraction correction function is used for all subjects, some residual postcorrection diffraction effects in the computed parameters are possible. Hence, three B-scans were done so that the transducer was focused at different depths (for the same horizontal scan) wherein, for one of them, the ROI was positioned at the transducer's focal zone and, for the other two, the ROIs were positioned above and below the focal zone by 1 mm. By this procedure, the computed parameters could be averaged over all the laterally and axially shifted scans. To summarize, the experiment consisted of a three-dimensional movement of the transducer to record several B-scans that were laterally and axially shifted, with each scan done according to the description in the preceding paragraph.

After the RF data were collected, B-scan images were created by computing the envelope using the Hilbert-transform approach. Custom-written programs in Matlab (The MathWorks, Inc., Natick, MA) were used for generating and displaying the images, and for computing the quantitative parameters described later.

Subjects and patch tests

A total of seven subjects with a clinical history of allergic contact dermatitis were recruited for the study. The subjects ranged in age from 25 to 66 years (mean = 41 years). Patch testing was performed with contact allergens (fragrance mix, wool alcohol and nickel sulphate) incorporated in petrolatum using Finn chambers (Epitest Ltd., Oy, Norway) affixed with Scanpor tape (Norgesplaster, Vennesla, Norway). Allergens were ap-

Table 2. Summary of US parameters studied in this work

Parameter	ROI
Skin thickness	Start of entry echo to the border between dermis and fat (epidermis and dermis)
Echogenicity (mean pixel amplitude expressed as a percentage of the full scale)	Upper dermis, extending from 0.225 mm to 0.450 mm from the skin surface
Attenuation coefficient slope	(a) Full dermis; (b) portion of the dermis corresponding to that of the normal skin
Echo statistics parameters: SNR, Weibull- b , K - α , GG- ν , and GG- c	Mid-dermis extending from 0.5 mm to 1 mm from the surface

plied for a period of 48 h to the ventral side of the forearm for 2 subjects, and to the thigh for 5 subjects. Imaging was performed 24 h after removal of the patches. Patch testing was also performed at nearby sites using 5% sodium lauryl sulphate to induce irritant contact dermatitis for the same seven patients. Similar to those at the allergic sites, the irritant patches were applied for 48 h and ultrasonic imaging was done 24 h after patch removal. Clinical grading of the reactions as 0, 1, 2, and 3 was performed at the time of imaging using standard clinical scoring scales used by the European and North American contact dermatitis groups. A higher value indicated a more severe reaction. Unaffected healthy sites were also imaged adjacent to the lesion sites. For control purposes, evaluation of a patch test site with petrolatum alone was also done for all subjects.

Ultrasound parameters

Table 2 provides a summary of the parameters studied in this work.

Skin thickness. The skin thickness was measured using the B-scan images displayed on the computer screen. It was taken to be the sum of the epidermal and dermal thicknesses, and was measured from the start of the entry echo to the interface between the dermis and subcutaneous fat. At the frequency used in this study (33 MHz), the epidermis and the entry echo could not be clearly separated. Because the interface between the dermis and fat was irregular, an average of several thickness values based on several scans and several locations within a particular scan was used. Typically, 16 measurements were used to compute the mean thickness. To compute thickness, the speed of sound was assumed to be 1.5 mm/ μ s for both the healthy and affected skin.

Echogenicity of upper dermis. Echogenicity refers to the mean pixel amplitude within an ROI, and is

proportional to the mean backscatter amplitude of the tissue within the useful frequency range. Even though this quantity is system-dependent (a different gain setting will lead to a different echogenicity value), it was simpler to compute than the frequency-dependent backscatter coefficient that we had studied earlier in healthy skin (Raju and Srinivasan 2001). To make this quantity non-dimensional, the pixel amplitudes were expressed as a percentage of the maximum signal amplitude that could be recorded by the system (500 mV for the setting used in our studies). Echogenicity values were computed for the upper dermis, which was taken to be the region from 225 μ m to 450 μ m below the start of the surface echo. To accurately determine the depth in the above manner, the location of the surface echo was computed for each echo line by a threshold detection procedure. The echogenicity values were corrected for diffraction effects using correction curves as described in the next section.

Attenuation coefficient slope. Attenuation coefficient at any given frequency is the rate of decay of US with the distance of propagation and is measured in units of dB/mm. Our previous studies have shown that within the 14 to 50 MHz range, the attenuation coefficient of skin tissues increases linearly with frequency (Raju and Srinivasan 2001). The slope of the attenuation coefficient vs. frequency curve is referred to as the attenuation coefficient slope (β), which is represented in units of dB/mm/MHz. Determining this quantity involves the computation of mean power spectra as a function of depth for several frequencies. At first, an ROI parallel to the skin surface and corresponding to the dermis was selected by the user by a visual examination of the B-scan image. The dermis was identified as the hyperechoic tissue lying above the hypoechoic fat. The ROI, which was initially an arbitrary quadrilateral (as the user picks four points), was modified into a parallelogram so as to have a uniform length in the axial direction at all the scan lines within the ROI. Each scan line within the ROI was then divided into several axial segments of 40 samples (200 ns), each with an overlap of 50% between the segments. The time duration of 200 ns corresponded to a thickness of 150 μ m, assuming a speed of sound of 1.5 mm/ μ s for the dermis. For a typical normal skin thickness of 1.2 mm, 15 such axial segments were available per scan line. In the lateral direction, a typical ROI of 4.0 mm consisted of 160 scan lines, each separated by 25 μ m. Power spectra corresponding to all the segments and scan lines were obtained by computing the Fourier transform after applying a Hamming window, and squaring the resultant. The segment length of 200 ns provided a frequency resolution of 5 MHz. Once power spectra were obtained, diffraction correction determined by the location of the center of each of the segments was applied

(see next section). Mean power spectra as a function of depth from the surface were computed by laterally averaging the diffraction-corrected power spectra from all the scan lines. Spectral slopes (dB/mm) representing the decay of US with depth were then computed for several frequencies in the range of 10 to 50 MHz. Finally, a linear fit to the spectral slope vs. frequency curve was computed to obtain the attenuation coefficient slope.

In the case of healthy skin tissues, the entire dermis was used to compute the attenuation coefficient slope. In the case of contact dermatitis, the thickness of the skin increased in many cases. In such cases, attenuation coefficient slopes were computed for both the full thickness of the dermis as well as for the smaller thickness corresponding to that of the healthy skin. In some of the affected sites, a subepidermal hypoechogenic band was seen. Including this band for the ROI did not affect the computed attenuation coefficient slopes significantly for cases analyzed in this work.

Echo statistics parameters. Ultrasonic signals can be modeled as stochastic signals because the precise details of the scattering structures in tissues and, consequently, the details of the backscattered signals are not known *a priori*. Support for stochastic modeling also comes from the fact that the US images of soft tissues have a random texture pattern termed speckle, similar to the appearance of a rough surface irradiated by a coherent laser source. In prior works, the first order statistics of the amplitude of backscattered signals from several tissues, such as the liver (Sommer *et al.* 1987), heart (Wear *et al.* 1986), breast (Shankar *et al.* 2001), eye (Romijn *et al.* 1991), and kidney (Wear *et al.* 1997), have been studied. Our previous studies on healthy skin tissues showed that the K, Weibull and generalized gamma (GG) distributions were able to model the envelope pdfs well (Raju and Srinivasan 2002). Accordingly, the echo statistics parameters studied in this work were the shape parameters of the K, Weibull and GG distributions fitted to the envelope data samples, as well as the SNR of echo envelope. The SNR is the ratio of mean to SD of the envelope data and is related to the number density of scatterers within the resolution cell (Tuthill *et al.* 1988). This quantity is also a measure of deviation from the Rayleigh statistics, which occurs when the resolution cell consists of a large number of randomly distributed scatterers. The SNR is equal to 1.91 when the Rayleigh conditions are satisfied, less than 1.91 for pre-Rayleigh conditions, and larger than 1.91 for post-Rayleigh or Rician conditions (Tuthill *et al.* 1988; Shankar 2000).

The shape parameters of the three distributions were determined by fitting pdfs to the envelope data using the

maximum likelihood (ML) method. The Weibull pdf is given by the following expression:

$$p(r) = \frac{b}{a} \left(\frac{r}{a}\right)^{b-1} e^{-\left(\frac{r}{a}\right)^b} \quad r \geq 0; a, b > 0 \quad (1)$$

The parameter b is referred to as the shape parameter because it determines the shape of the pdf, whereas the parameter a is simply a scaling parameter. By suitably changing the values of the parameter b , the Weibull distribution can be made to model pre-Rayleigh ($b < 2$), Rayleigh ($b = 2$) or Rician ($b > 2$) conditions. Hence, the parameter b can also be seen to be a measure of deviation from the Rayleigh condition. To estimate this parameter, the log-likelihood function was first obtained:

$$L(r_1, r_2, \dots, r_N, a, b) = N \ln b - (b - 1) \sum \ln r_i - \sum \left(\frac{r_i}{a}\right)^b - Nb \ln a \quad (2)$$

In the above expression, r_i represents an envelope sample, N represents the number of samples, and the summation is over all the samples. By setting the first partial derivative of the log-likelihood function with respect to a to zero, the following relationship between the parameters a and b is obtained:

$$a = \left(\frac{\sum r_i^b}{N}\right)^{1/b} \quad (3)$$

With the above relationship, a simple one-dimensional (1-D) exhaustive search method was used to obtain the ML solution: A sufficiently large grid of solution points for the parameter b was first chosen and the corresponding values for the parameter a were computed using eqn (3). The log-likelihood function was computed at the points (a, b) , and the one corresponding to the maximum was taken to be the solution. Further refinement around the solution point was then done to improve the accuracy of the estimates.

The K distribution has been previously studied in modeling US echo signals from the breast and liver (Molthen *et al.* 1998). Its pdf is given by:

$$p(r) = 2 \left(\frac{r}{2}\right)^{\alpha} \frac{b^{\alpha+1}}{\Gamma(\alpha)} K_{\alpha-1}(br), \quad r \geq 0; \alpha, b > 0 \quad (4)$$

The parameter α is the shape parameter, and can be identified as an effective scatterer number density (Narayanan *et al.* 1994). Its value can range from zero to

infinity. When its value approaches infinity, the K distribution approaches the Rayleigh distribution. To obtain the maximum likelihood solution, the log-likelihood function was obtained:

$$L(r_1, r_2, \dots, r_N, b, \alpha) = N \left[(\alpha + 1) \ln(b) - \ln \left(\frac{\Gamma(\alpha)}{2} \right) \right] + \alpha \sum \ln \left(\frac{r_i}{2} \right) + \sum \ln (K_{\alpha-1}(br_i)). \quad (5)$$

Because the partial derivatives of the above expression are difficult to compute, a 2-D Nelder-Mead simplex optimization method available in the Matlab's Optimization toolbox was used to obtain the ML solution as described in our earlier work (Raju and Srinivasan 2002).

The GG pdf is given by the following expression

$$p(r) = \frac{c r^{(c\nu-1)}}{a^{c\nu} \gamma(\nu)} e^{-\left(\frac{r}{a}\right)^c}, \quad r \geq 0, a, \nu, c > 0 \quad (6)$$

In the above expression, a is the scaling parameter and ν and c are two parameters that determine the shape of the pdf. In particular, the parameters ν and c are capable of adjusting more or less independently, the lower and upper tails of the pdf, respectively (Coulson et al. 1998; Shankar 2001). The GG distribution has several other distributions as special cases: Rayleigh ($c = 2, \nu = 1$), exponential ($c = 1$ and $\nu = 1$), Nakagami ($c = 2$), Weibull ($\nu = 1$) and also the usual gamma ($c = 1$) distribution. Although no physical explanation seems to be available, the GG distribution has been found to be more useful in modeling envelope signals from skin tissues than many other distributions (Raju and Srinivasan 2002). In addition, it provides two parameters for characterizing tissues as opposed to one for the Weibull and K distributions. To compute its shape parameters, the log-likelihood function was first obtained:

$$L(r_1, r_2, \dots, r_N, a, \nu, c) = N \ln c - (c\nu - 1) \sum \ln r_i - \sum \left(\frac{r_i}{a} \right)^c - Nc\nu \ln a - N \ln \Gamma(\nu). \quad (7)$$

By setting the first partial derivatives of the above expression with respect to c and a to zero, we get (Wingo 1987):

$$\nu = - \left\{ c \left(\frac{\sum \ln r_i}{N} - \frac{\sum r_i^c \ln r_i}{\sum r_i^c} \right) \right\}^{-1} \quad (8)$$

$$a = \left(\frac{\sum r_i^c}{N\nu} \right)^{1/c} \quad (9)$$

The ML solution was obtained using a 1-D exhaustive search method similar to the one described for the Weibull pdf. First, a large solution grid was assumed for the parameter c , and the corresponding values for ν and a were obtained using eqns (8) and (9). The likelihood expression was then evaluated at the points (a, ν, c) , and the one corresponding to the maximum was selected. Further refinement around the solution point was then done to improve the accuracy of the estimates.

For computing the above echo statistics parameters, a region-of-interest (ROI) corresponding to the dermis from 0.5 to 1 mm below the skin surface was chosen. The reason for choosing only 0.5 mm for the ROI was to keep the length small enough to minimize both attenuation and diffraction effects within the ROI (although diffraction correction is applied based on the overall location of the ROI). The envelope samples corresponding to the scan lines within this ROI were collected to form empirical histograms. When combining the data, only every other scan line and every fourth sample along a scan line were used due to the correlated nature of adjacent data samples. The spacing between the samples roughly corresponded to one half of the lateral and axial resolutions. Typically, a total of about 1600 samples were available for constructing envelope histograms. After the parameters were estimated as described above, a correction for diffraction was applied to the parameters, depending on the location of the center of the ROI (next section). It should also be pointed out that, for a given envelope data, the parameters SNR, Weibull- b , and K - α are not independent of one another. However, their dynamic ranges are different and, hence, all of them were computed and studied in this work.

Statistics

The parameters computed for the affected sites (both allergic and irritant contact dermatitis considered as one population, which will be referred to as the "affected sites") were compared against healthy skin tissues using the Wilcoxon sign rank test. P values to test if the difference in the values were significantly different from zero were computed (paired test). A value of $p < 0.05$ was considered to be significant.

DIFFRACTION CORRECTION

The use of focused transducers requires compensation for diffraction effects when computing quantitative tissue characterization parameters. Due to variation in the beam amplitude with distance, diffraction affects power spectra measurements and, consequently, the attenuation coefficient slope. Diffraction also affects the echo statistics parameters due to variation in the beam size with distance. For instance, at the focus, the beam

size is small and, hence, a smaller number of scatterers contribute to the resultant, leading to smaller SNR values. However, away from the focus, the beam is broader and, hence, a larger number of scatterers contribute to the resultant, leading to larger SNR values. To compensate for diffraction, various approaches, both theoretical and experimental, have been proposed in the literature. In our previous studies (Raju and Srinivasan 2001, 2002), the transducer was axially translated so as to shift the location of the focal zone to a particular depth of interest. In such experiments, a correction is not required because data are always obtained from the transducer focal zone. However, such a technique was found to be less preferable in a clinical setting due to the increased time of imaging. Hence, it was decided to make corrections for the diffraction effects using empirical correction curves obtained using human dermal tissues *in vivo*.

The basic premise in determining the correction curves was that, if the same tissue was placed at different distances from the transducer, then any parameter being computed (*e.g.*, power spectrum at a particular frequency, SNR, Weibull-*b* *etc.*) must be the same at all the locations after diffraction compensation is applied. Therefore, the correction curves can be obtained experimentally by determining the parameter of interest for the various tissue locations. For this purpose, five subjects who were all different from the ones who participated in patch testing were recruited. Data were collected at the dorsal forearm for 19 locations spaced apart by 0.25 mm through axial translation of the transducer. Two repetitions were done for all the subjects. Figure 1 illustrates the images obtained for one subject when the tissue was at three of the 19 locations. For each of the 19 images, two sets of ROIs, one for studying variations in mean spectra with depth, and the other for studying the variation in echo statistics parameters with depth, were selected. The former ROI spanned a distance of 60 samples or 0.225 mm in the axial direction and the latter spanned a distance of about 0.5 mm in the axial direction. The mean spectra, echogenicity, SNR, Weibull-*b*, *K*- α , GG- ν and GG-*c* parameters were computed for all the 19 locations as described in the previous section.

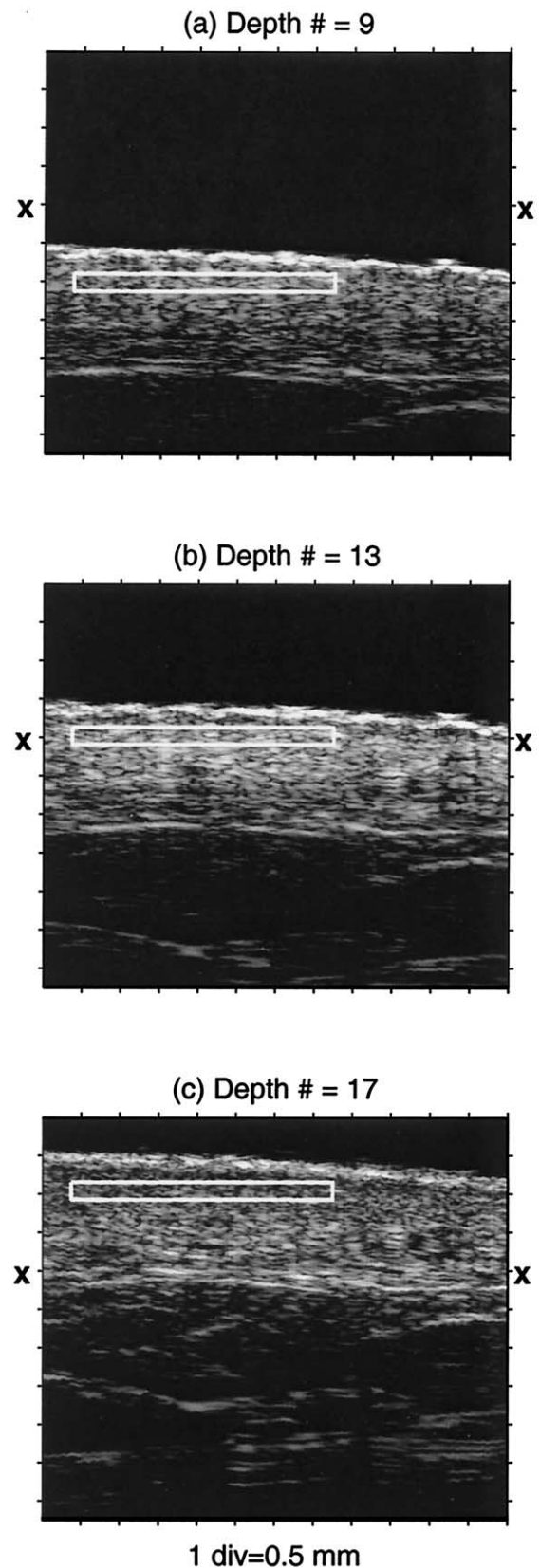


Fig. 1. Experiments to determine diffraction correction curves. US data were collected from skin *in vivo* when the tissue was at several depths separated by 0.25 mm. The figure shows three such depths, one each corresponding to the ROI being (a) below the focus, (b) at the focus and (c) above the focus. (x) = location of the transducer's focal zone. The ROIs in the images were used to compute mean power spectra at various distances from the transducer. Another set of ROIs, larger than the above, were used to determine the correction curves for the echo-statistics parameters.

Figure 2 shows the diffraction correction curves for power spectra at three frequencies over a distance of 1.5 mm on either side of the focus. It can be seen that the correction curve has a narrower width at higher frequencies, which is consistent with the fact that the higher frequencies are more tightly focused. For comparison, theoretical diffraction correction curves developed by Chen et al. (1997) are also shown. Their theoretical correction curve was based on a rigorous treatment of the physics of acoustic wave propagation, and took into account the transducer geometry and frequency characteristics. In their work, mathematical formulas were also provided for two special cases, namely, the flat disk and spherically focused transducers. Their theoretical and our empirical correction curves agree very well at lower frequencies. At higher frequencies the empirical curve is seen to be broader than the theoretical curve. One reason for this could be due to using a finite length for both the segment length in computing the power spectrum (0.225 mm) and for sampling the curves (0.25-mm apart). These two effects tend to smear the correction curves, the effects of which are more prominent for the higher frequencies. During analysis of data collected from patients, the computed power spectra were corrected for diffraction effects by dividing them by correction functions at the appropriate distance. The attenuation coefficients were then computed using the corrected power spectra.

Figure 3 shows the computed diffraction correction curves for the echo statistics parameters. The SNR generally increases with distance from the focus. This is to be expected because, away from the focus, the beam becomes broader and, therefore, a larger number of scatterers contribute to the resultant. The increase in the number of scatterers pushes the envelope pdf closer to the Rayleigh pdf and the SNR approaches 1.91. The location of the minimum point of SNR, however, does not match the location of the focus, but is seen to be deeper. The reason for this is not clear, but is probably due to the fact that the dermal tissue scatterers are not uniformly dense within the 0.5-mm ROI, and that the variations in amplitude of the beam within this 0.5 mm affect the echo statistics in a complex way. A similar trend is seen for the Weibull- b and K - α parameters. The Weibull- b curve is similar to the SNR curve, which is due to the fact that the two quantities are approximately linearly related over the limited range of values obtained. The K - α parameter becomes large as we move away from the focus, which is a consequence of the envelope pdf approaching the Rayleigh pdf. The percentage variability in its estimates is larger than that for the other parameters, which is due to the fact that a very large sample size is needed to estimate the parameter even for moderately large values of α . The GG- ν curve shows a trend that is opposite to that of the SNR,

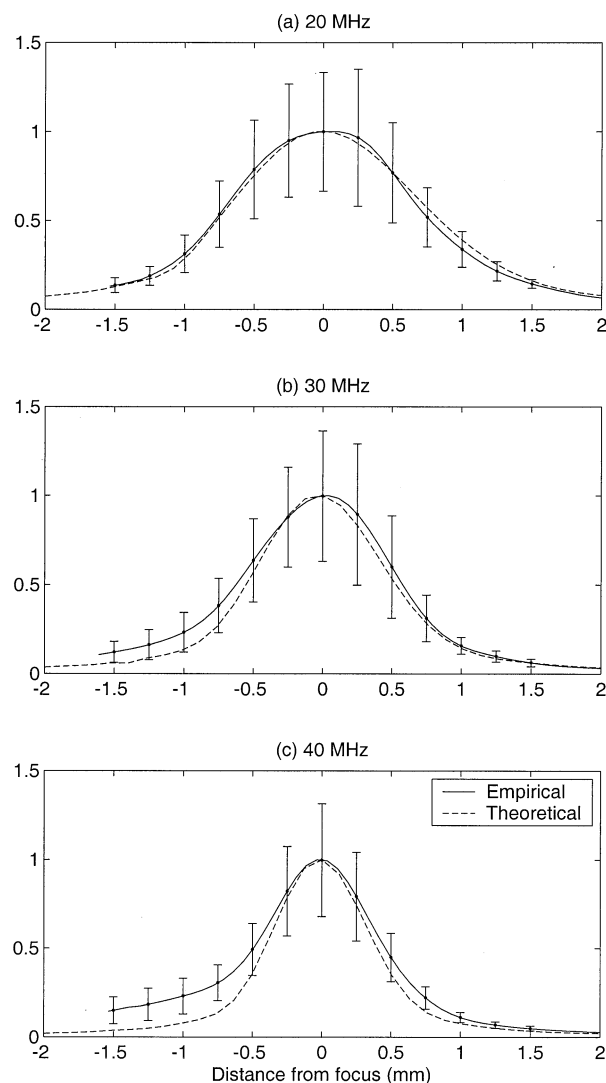


Fig. 2. Diffraction correction curves (in linear units) for correcting power spectra as a function of the distance from the focus, obtained using human dermal tissues *in vivo*. The solid line (—) is the mean correction curve from 10 experiments (5 subjects, 2 repetitions each); error bars indicate the SDs; the dashed line (---) is based on the theoretical formulation developed by Chen et al. (1997).

Weibull- b and K - α parameters and the GG- c parameter shows a trend that is similar to the above parameters. The mean correction curves for all the parameters were normalized so as to have a minimum value of unity for all the parameters except the GG- ν , which was normalized to have a maximum value of unity. These normalized curves constituted the diffraction correction curves for the various echo statistics parameters. Diffraction correction functions were also determined for the echogenicity parameter in the above manner (not shown).

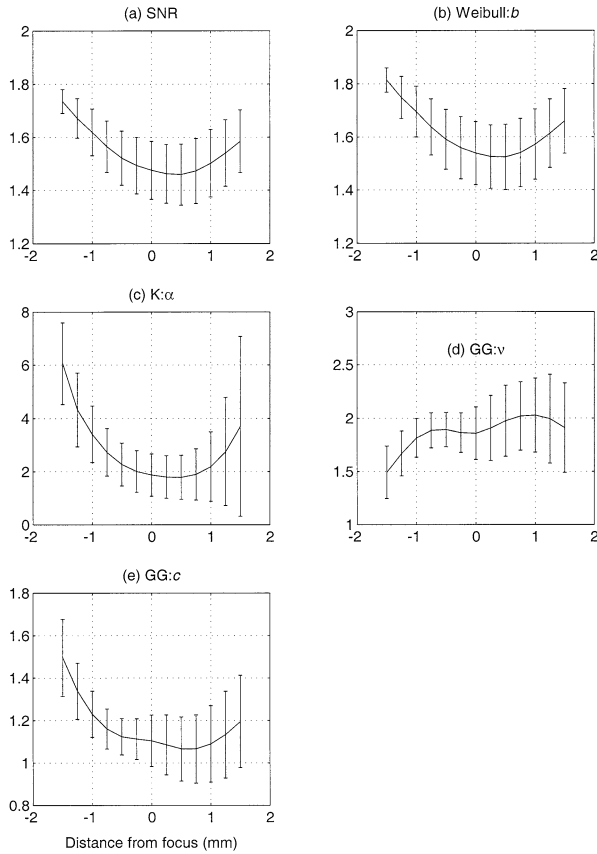


Fig. 3. Diffraction correction curves for correcting estimates of echo-statistics parameters as a function of the distance from the focus, obtained using human dermal tissues *in vivo*. The solid line (—) is the mean correction curve from 10 experiments (5 subjects, 2 repetitions each); error bars indicate the SDs. The increase in SNR away from the focus indicates that the envelope pdf approaches the Rayleigh pdf.

It should also be emphasized that the diffraction corrections for the SNR and pdf shape parameters are only valid within a limited range of values. To apply the correction curves to the echo-statistics parameters, the scattering conditions need to be pre-Rayleigh after correction is applied. For example, if the diffraction correction in Fig. 3b is used for a tissue that already shows Rayleigh statistics at the focus (SNR = 1.91), the compensated values when the ROI is away from the focus would be larger than 1.91, which is incorrect because the increased beam size should still result in Rayleigh conditions. In this work, all the computed values for both the healthy tissues and affected sites were pre-Rayleigh even after the application of correction functions and, hence, the correction procedure was valid.

To verify the diffraction correction procedure, data were collected from one additional subject who was different from those used in obtaining the correc-

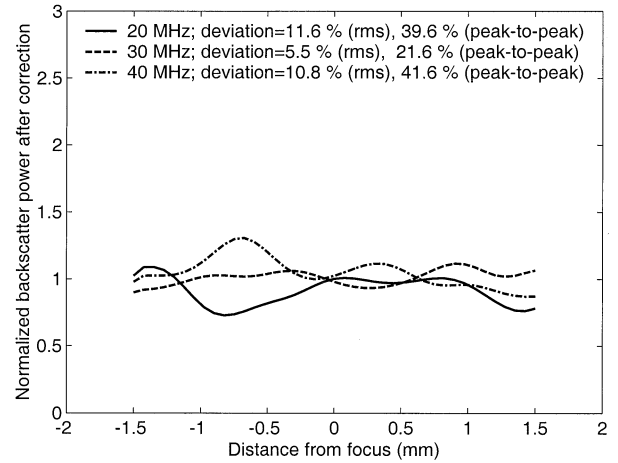


Fig. 4. Corrected power spectra for one subject as a function of the distance from the focus. The deviations are expressed as a percentage of the mean values.

tion curves. All the ultrasonic parameters were computed and corrected for diffraction effects. Figure 4 shows the power spectra at 20, 30 and 40 MHz as a function of distance from the focus. Comparing Figs. 2 and 4, it can be seen that the correction has resulted in a more uniform distribution of the power spectra. The variability in the results could be attributed to the finite number of scan lines used in computing the mean power spectra. The variability in the corresponding attenuation coefficient slope would be smaller due to the linear fit of the power spectrum vs. frequency curve, which tends to smooth the variations. In practice, the variability was further minimized through averaging the computed attenuation coefficient slopes obtained from several scans, both axial and lateral. Figure 5 shows the corrected echo statistics parameters as a function of the distance from the focus. Comparing Figs. 3 and 5, it can be seen that the diffraction correction to these parameters has resulted in a more uniform distribution of the parameters with distance. The variability is seen to be the highest for the K - α parameter.

RESULTS

Figure 6 shows an image of healthy skin tissue and skin affected by allergic contact dermatitis for one subject. It can be seen that the skin thickness increased significantly for the case of contact dermatitis. It can also be seen that, in the case of the affected skin, the amplitude of the pixels in the upper dermis decreases. Figure 7 shows the differences in skin thickness measurements for two cases: (1) between the petrolatum control site and the corresponding healthy site and (2)

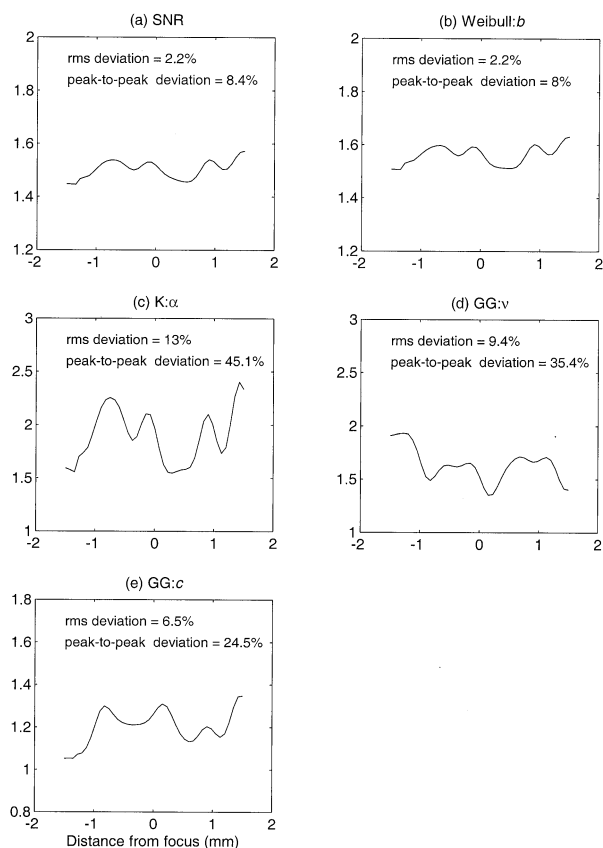


Fig. 5. Corrected echo-statistics parameters for one subject as a function of the distance from the focus. The deviations are expressed as a percentage of the mean values.

between the affected site and the corresponding healthy site. Data from all subjects, irrespective of whether changes were clinically observed or not, were used. A significant increase in the skin thickness can be seen at the affected site. The petrolatum control site

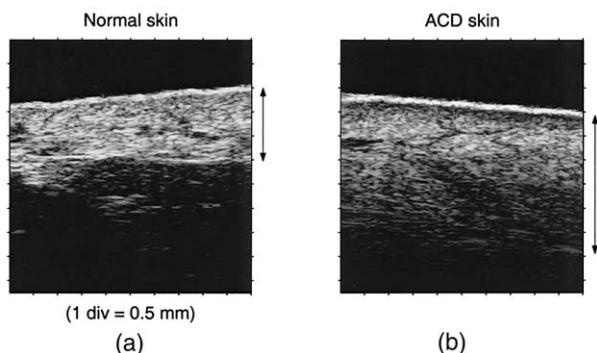


Fig. 6. Images of (a) healthy skin and (b) allergic contact dermatitis (ACD) in the thigh region of a 28-year-old woman. The extent of the dermis is shown by the arrows. The increased thickness in the case of contact dermatitis can be seen. The normal skin was adjacent to the ACD site.

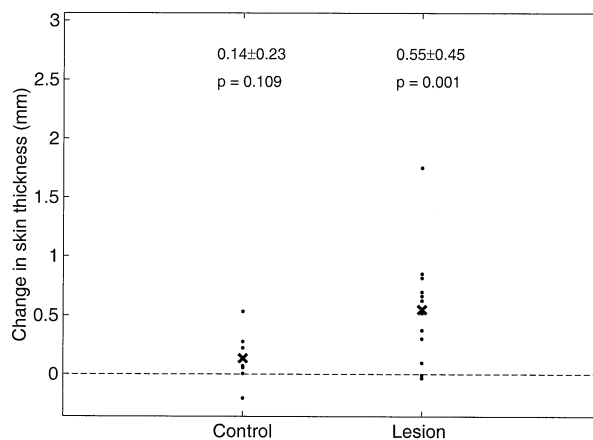


Fig. 7. Difference in skin thickness between the petrolatum control site and the corresponding healthy site (“Control”); and between the affected site and the corresponding normal site (“Lesion”). The dots (•) indicate the difference in the respective values for each subject; the (×) indicates the mean across all subjects. The text in the figure refers to mean \pm SD (first row) and the *p* values (second row).

also showed a slight, but not statistically significant, increase in skin thickness.

Figure 8 shows the differences in the echogenicity of the upper dermis for the two cases mentioned above. The echogenicity at the affected sites was significantly smaller than those at the healthy sites. Figure 9 shows the results for the attenuation coefficient slope. In general, since the skin thickness increased for the affected sites, the attenuation coeffi-

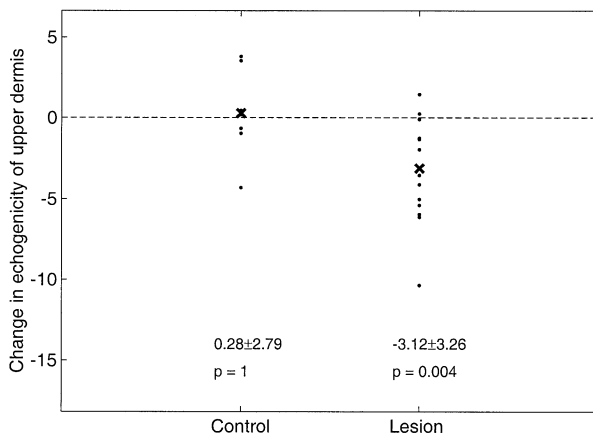


Fig. 8. Difference in echogenicity of the upper dermis between petrolatum control site and the corresponding healthy site (“Control”); and between the affected site and the corresponding healthy site (“Lesion”). The dots (•) indicate the difference in the respective values for each subject; the (×) indicates the mean across all subjects. The text in the figure refers to mean \pm SD (first row) and the *p* values (second row).

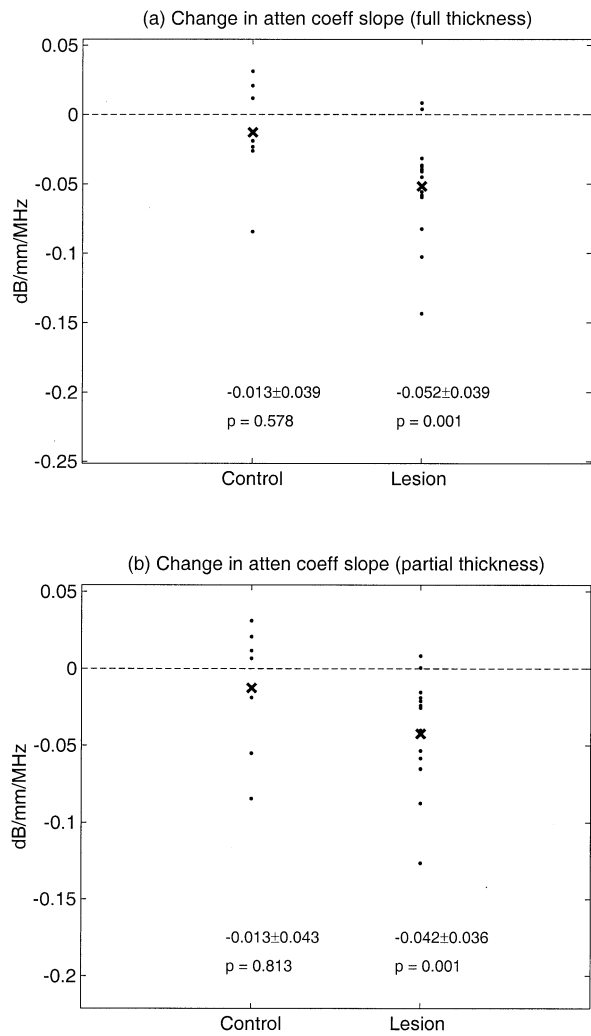


Fig. 9. Difference in attenuation coefficient slope between the petrolatum control site and the corresponding healthy site (“Control”); and between the affected site and the corresponding healthy site (“Lesion”). The dots (\cdot) indicate the difference in the respective values for each subject; the (\times) indicates the mean across all subjects. The text in the figure refers to mean \pm SD (first row) and the p values (second row). The top panel is when the entire dermal thickness was used in computing the attenuation coefficient slope. The bottom panel is when only the dermal thickness corresponding to that of the healthy skin was used in computing the attenuation coefficient slope.

cient slopes were computed for both the full thickness of the lesion and for the partial thickness corresponding to that of the healthy skin. In both cases, the affected skin showed a significant decrease in the attenuation coefficient slope. Figure 10 shows the results for the echo-statistics parameters. Although slight increases in the mean values could be seen for all the parameters except for the GG- ν parameter, for which a decrease was seen, the differences were not statistically significant. Among the various param-

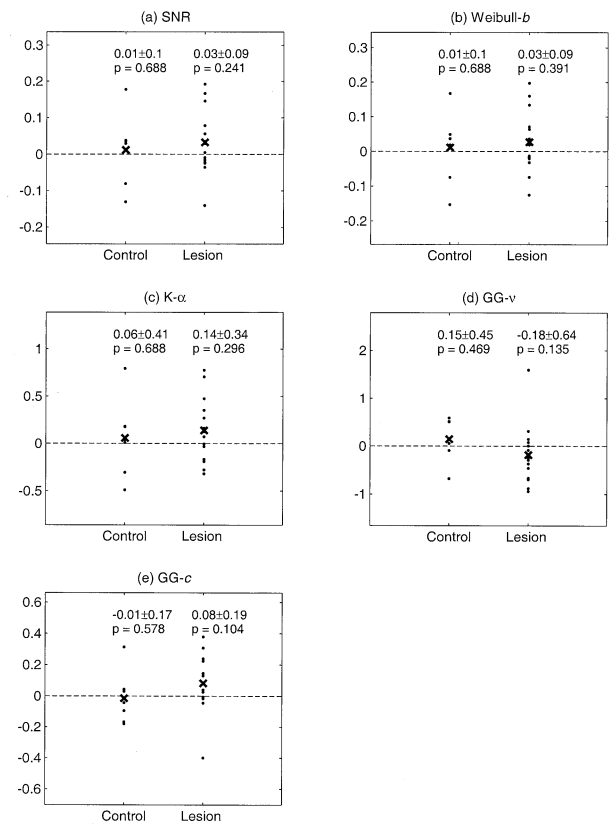


Fig. 10. Difference in echo statistics parameters between the petrolatum control site and the corresponding healthy site (“Control”); and between the affected site and the corresponding healthy site (“Lesion”). The dots (\cdot) indicate the difference in the respective values for each subject; the (\times) indicates the mean across all subjects. The text in the figure refers to mean \pm SD (first row) and the p values (second row).

ters, the GG- ν and GG-c parameters were seen to perform relatively better in that their p values were smaller than those of the others.

DISCUSSION

Diffraction correction

In this work, quantitative methods for characterizing skin tissues were presented. In particular, methods to compute parameters without the influence of diffraction effects were developed. One method to minimize diffraction effects is to record multiple B-scans by axially moving the transducer between the scans. However, during preliminary work leading to this study, it was found that motion artefacts made it very difficult to combine multiple B-scans taken after axially shifting the transducer. In general, it was not possible for the patient to hold still for more than a few seconds during the experiment. For instance, depending on the body site being

Table 3. Summary of computed parameters

	Healthy	Lesion (all scores)	Lesion (excluding zero scores)
Thickness (mm)	1.44 (0.25)	1.99 (0.45)*	2.15 (0.45)*
Upper dermis echogenicity	11.3 (3.2)	8.1 (3.0)*	6.7 (2.1)*
Full thickness β (dB/mm/MHz)	0.201 (0.051)	0.149 (0.040)*	0.130 (0.023)*
Partial thickness β (dB/mm/MHz)	0.201 (0.051)	0.158 (0.028)*	0.147 (0.015)*
SNR	1.361 (0.072)	1.393 (0.067)	1.400 (0.072)
Weibull- <i>b</i>	1.424 (0.076)	1.451 (0.072)	1.459 (0.076)
<i>K</i> - α	1.244 (0.293)	1.382 (0.318)	1.430 (0.321)
GG- ν	2.342 (0.465)	2.162 (0.668)	2.189 (0.637)
GG- <i>c</i>	0.939 (0.109)	1.021 (0.161)	1.014 (0.166)

Comparison of estimated parameters for healthy skin and affected skin. The values indicated are mean (SD). For attenuation coefficient slope β , two values were computed, one corresponding to the full thickness of the lesion, and the other corresponding to the thickness of the healthy skin (excluding the epidermis). * Statistically significant difference from healthy site at a 0.05 significance level.

imaged and the posture of the patient during the experiment, normal breathing motion could pose a challenge to hold the tissue still. Therefore, the total duration of imaging must be as short as possible. The experiments to determine the diffraction correction were performed with prior planning to hold the tissue still, which was not possible in a practical sense with patients. With the methods presented in this work, only a single B-scan image is needed and there is no need to move the transducer toward the tissue, thereby reducing imaging time and making quantitative studies possible (more B-scans may be used for averaging purposes).

Quantitative characterization of contact dermatitis

Contact dermatitis was studied as an example because of the ease of patch testing methods. Table 3 summarizes the results from this work for all the parameters studied. A significant increase in skin thickness, decrease in echogenicity of the upper dermis and decrease in attenuation coefficient slope were found at the affected sites. Previous researchers using lower frequency US have also concluded that the skin thickness increases in the case of contact dermatitis (Serup et al. 1984; Serup and Staberg 1987; Seidenari and Di Nardo 1992). In measuring the skin thickness, the same speed of sound was used for both the normal and affected skin, both in our study and the earlier studies on contact dermatitis. Another study using SLAM at 100 MHz indicated a small but significant decrease in the speed of sound in the dermis with increasing water content (Olerud et al. 1987). Therefore, it is possible that some of the observed increase in skin thickness could be due to a decrease in sound speed at the affected sites. However the increase in skin thickness measured in our studies was quite high (thickness sometimes doubled) and it is likely that the skin thickness, indeed, increases at the affected sites. Moreover, other studies using caliper measurements have shown that the skin thickness, increases

in the case of allergic and irritant reactions (Wahlberg 1983; Przybilla et al. 1984; Wahlberg 1993).

Our results agree with earlier results based on 20-MHz US (Seidenari and Belletti 1998) that alterations occurring at the papillary dermis decrease the echogenicity in this region. Our study seems to be the first where the attenuation coefficient slope has been calculated for skin affected by contact dermatitis. The attenuation coefficient slope at the affected sites was $75\% \pm 16\%$ (mean \pm SD) of that of the healthy skin. When the sites that did not show any clinical reactions were excluded (cases corresponding to zero scores), the attenuation coefficient slope was $68\% \pm 10\%$ of that of healthy skin. A possible reason for the decrease in attenuation coefficient slope at the affected sites could be that the dermis expands due to edema and is filled by fluids, thereby increasing the water content. Previous studies at 100 MHz have shown that attenuation is inversely related to water content (Olerud et al. 1987). Therefore, the increase in water content in the affected areas would then lead to a decrease in the attenuation coefficient.

Our previous study on echo statistics showed that the Weibull, *K* and GG pdfs were capable of modeling the statistical fluctuations of the envelope of backscatter signals from skin tissues (Raju and Srinivasan 2002). In the present study, the parameters of these pdfs were computed at an ROI that spanned from 0.5 to 1 mm from the skin surface. The aim was to determine if there were changes to the mid-dermis that could be registered by these parameters. However, the results showed no significant differences between the affected sites and the healthy skin. This is surprising because, due to edema, the density of scatterers could be expected to decrease because the same set of scatterers would occupy a larger thickness. Consequently, the SNR could be expected to decrease. The results of the present study indicate that the edema formation might be localized to the upper dermis or that any changes in the density of scatterers is

not sufficient enough to cause significant changes in the echo-statistics parameters in the region 0.5 to 1 mm below the surface. In general, the determination of echo statistics parameters was not as easy as the attenuation coefficient. This is because the presence of inhomogeneities such as hair follicles affect the echo statistics more significantly than the attenuation coefficient.

In this study, both the allergic and irritant reactions were considered together as one population. It is possible that any genuine differences in the computed parameters between the allergic and irritant sites contribute to the variability seen in the results. Future work could study if significant differences between the allergic and irritant reactions are observed for the ultrasonic tissue characterization parameters. Also, other noninvasive methods, such as transepidermal water loss measurements and confocal imaging parameters (Gonzalez *et al.* 1999) could be combined with ultrasonic tissue parameters to characterize skin lesions, such as contact dermatitis.

General comments on quantitative ultrasonic studies of skin

Our studies support the hypothesis that quantitative studies of the skin might add useful information to conventional B-scan imaging. For instance, the fact that the attenuation coefficient slope decreases in contact dermatitis cannot be determined solely based on the B-scan images. Whether the additional information has significant diagnostic capability or not remains to be seen. At present, it appears that quantitative tissue characterization studies are an addition to, and not a replacement for, conventional ultrasonic imaging. Even in our quantitative studies, B-scan images were always used to identify a uniform ROI within which the parameters could be computed. Moreover, our study shows that, although some parameters can differentiate contact dermatitis from healthy skin (*e.g.*, attenuation coefficient slope), other parameters cannot (*e.g.*, echo statistics). Therefore, it appears that a combination of several parameters might be needed for reliable ultrasonic characterization.

An important goal of future quantitative studies of the skin would be to distinguish between benign and malignant lesions. The distinction between benign and malignant tissues occurs at cellular and subcellular levels (*e.g.*, increased size of nuclei in malignant lesions). For such applications, quantitative studies at even higher frequencies (100 MHz) might have good potential in tissue characterization because the domain of scattering from cellular structures is approached at such frequencies. Support for this hypothesis comes from imaging studies at 100 MHz where the internal structures of tumors were better visualized than at lower frequencies (Passmann and Ermert 1996). Additional support comes from *in vitro* acoustic microscopy of skin specimens at

600 MHz where specific diagnosis of cutaneous neoplasms and inflammatory cutaneous conditions seems to be possible (Barr *et al.* 1991). The methods presented in this work could serve as a foundation for quantitative studies at even higher frequencies.

Acknowledgments—The work reported here was supported in part by a grant in Aid of Research from the National Academy of Sciences through Sigma Xi. The authors thank Dr. Sui ren Wan for his help in computing the theoretical diffraction correction function, and to the anonymous reviewers for their useful comments.

REFERENCES

- Barr RJ, White GM, Jones JP, Shaw LB, Ross PA. Scanning acoustic microscopy of neoplastic and inflammatory cutaneous tissue specimens. *J Invest Dermatol* 1991;96:38–42.
- Chen X, Phillips D, Schwartz KQ, Mottley JG, Parker KJ. The measurement of backscatter coefficient from a broadband pulse-echo system: A new formulation. *IEEE Trans Ultrason Ferroelect Freq Control* 1997;44:515–525.
- Coulson AJ, Williamson AG, Vaughan RG. Improved fading distribution for mobile radio. *IEEE Proc Communic* 1998;145:197–202.
- Fornage BD, McGavran MH, Duvic M, Waldron CA. Imaging of the skin with 20-MHz US. *Radiology* 1993;189:69–76.
- Foster FS, Pavlin CJ, Harasiewicz KA, Christopher DA, Turnbull DH. Advances in ultrasound biomicroscopy. *Ultrasound Med Biol* 2000; 26:1–27.
- Fournier C, Bridal SL, Berger G, Laugier P. Reproducibility of skin characterization with backscattered spectra (12–25 MHz) in healthy subjects. *Ultrasound Med Biol* 2001;27:603–610.
- Gniadecka M, Jemec GBE. Quantitative evaluation of chronological ageing and photoageing in vivo: Studies on skin echogenicity and thickness. *Br J Dermatol* 1998;139:815–821.
- Gonzalez S, Gonzalez E, White WM, Rajadhyaksha M, Anderson RR. Allergic contact dermatitis: Correlation of *in vivo* confocal imaging to routine histology. *J Am Acad Dermatol* 1999;40:708–713.
- Guittet C, Ossant F, Vaillant L, Berson M. *In vivo* high frequency ultrasonic characterization of human dermis. *IEEE Trans Biomed Eng* 1999;46:740–746.
- Harland CC, Kale SG, Jackson P, Mortimer PS, Bamber JC. Differentiation of common benign pigmented skin lesions from melanoma by high-resolution ultrasound. *Br J Dermatol* 2000;143: 281–289.
- Insana MF, Wagner RF, Gara BS, Brown DG, Shawker TH. Analysis of ultrasound image texture via generalized Rician statistics. *Opt Eng* 1986;25:743–748.
- Madsen EL. Method of determination of acoustic backscatter and attenuation coefficients independent of depth and instrumentation. In: Shung KK, Thieme GA, eds. *Ultrasonic scattering in biological tissues*. Boca Raton, FL: CRC Press, 1993:205–249.
- Molthen RC, Shankar PM, Reid JM, *et al.* Comparisons of the Rayleigh and K-distribution models using *in vivo* breast and liver tissue. *Ultrasound Med Biol* 1998;24:93–100.
- Narayanan VM, Shankar PM, Reid JM. Non-Rayleigh statistics of ultrasonic backscattered signals. *IEEE Trans Ultrason Ferroelect Freq Control* 1994;41:845–852.
- Olerud JE, O'Brien W, Riederer-Henderson MA, *et al.* Ultrasonic assessment of skin and wounds with the scanning laser acoustic microscope. *J Invest Dermatol* 1987;88:615–623.
- Ophir J, Mehta D. Elimination of diffraction error in acoustic attenuation estimation via axial beam translation. *Ultrason Imaging* 1988; 10:139–152.
- Passmann C, Ermert H. A 100-MHz ultrasound imaging system for dermatologic and ophthalmologic diagnostics. *IEEE Trans Ultrason Ferroelect Freq Control* 1996;43:545–552.

- Przybilla B, Ring J, Schmid JG. Comparison of methods for macroscopic assessment of epicutaneous allergic contact reactions in guinea pigs. *Contact Derm* 1984;11:229–235.
- Raju BI, Srinivasan MA. High-frequency ultrasonic attenuation and backscatter coefficients of *in vivo* normal human dermis and subcutaneous fat. *Ultrasound Med Biol* 2001;27:1543–1556.
- Raju BI, Srinivasan MA. Statistics of envelope of high frequency ultrasonic backscatter from human skin *in vivo*. *IEEE Trans Ultrason Ferroelect Freq Control* 2002;49:871–882.
- Robinson DE, Wilson LS, Bianchi T. Beam pattern (diffraction) correction for ultrasonic attenuation measurement. *Ultrason Imaging* 1984;6:293–303.
- Romijn RL, Thijssen JM, Oosterveld BJ, Verbeek AM. Ultrasonic differentiation of intraocular melanomas: Parameters and estimation methods. *Ultrason Imaging* 1991;13:27–55.
- Seidenari S, Belletti B. The quantification of patch test responses: A comparison between echographic and calorimetric methods. *Acta Derm-Vener* 1998;78:364–366.
- Seidenari S, Di Nardo A. Cutaneous reactivity to allergens at 24-h increases from the antecubital fossa to the wrist: An echographic evaluation by means of a new image analysis system. *Contact Derm* 1992;26:171–176.
- Serup J, Staberg B. Ultrasound for assessment of allergic and irritant patch test reactions. *Contact Derm* 1987;17:80–84.
- Serup J, Staberg B, Klemp P. Quantification of cutaneous oedema in patch test reactions by measurement of skin thickness with high-frequency pulsed ultrasound. *Contact Derm* 1984;10:88–93.
- Shankar PM. A general statistical model for ultrasonic backscattering from tissues. *IEEE Trans Ultrason Ferroelect Freq Control* 2000;47:727–736.
- Shankar PM. Ultrasonic tissue characterization using a generalized Nakagami model. *IEEE Trans Ultrason Ferroelect Freq Control* 2001;48:1716–1720.
- Shankar PM, Dumane VA, Reid JM, et al. Classification of ultrasonic B-mode images of breast masses using Nakagami distribution. *IEEE Trans Ultrason Ferroelect Freq Control* 2001;48:569–580.
- Shung KK, Thieme GA. *Ultrasonic scattering in biological tissues*. Boca Raton, FL: CRC Press, 1993.
- Sommer G, Stern R, Chen H. Cirrhosis. US Images with narrow band filtering. *Radiology* 1987;165:425–430.
- Turnbull DH, Starkoski BG, Harasiewicz KA, et al. A 40–100 B-scan ultrasound backscatter microscope for skin imaging. *Ultrasound Med Biol* 1995;21:79–88.
- Tuthill TA, Sperry RH, Parkar KJ. Deviations from Rayleigh statistics in ultrasonic speckle. *Ultrason Imaging* 1988;10:81–89.
- Wahlberg JE. Assessment of skin irritancy: Measurement of skin fold thickness. *Contact Derm* 1983;9:21–26.
- Wahlberg JE. Measurement of skin-fold thickness in the guinea pig. Assessment of edema-inducing capacity of cutting fluids, acids, alkalis, formalin and dimethyl sulfoxide. *Contact Derm* 1993;23:141–145.
- Wear KA, Shoup TA, Popp RL. Ultrasonic characterization of canine myocardium contraction. *IEEE Trans Ultrason Ferroelect Freq Control* 1986;33:347–353.
- Wear KA, Wagner RF, Brown DG, Insana MF. Statistical properties of estimates of signal-to-noise ratio and number of scatterers per resolution cell. *J Acoust Soc Am* 1997;102:635–641.
- Wingo DR. Computing maximum-likelihood parameter estimates of the generalized gamma distribution by numerical root isolation. *IEEE Trans Reliability* 1987;36:586–590.